

Measurement of the $e^+e^- \rightarrow$ hadrons cross-section at low energy with ISR events at BABAR

B. MALAESCU^a *

On behalf of the BABAR Collaboration

^aLaboratoire de l'Accélérateur Linéaire,
IN2P3/CNRS, Université Paris-Sud 11, Orsay, France

The precise measurement of the cross section $e^+e^- \rightarrow \pi^+\pi^-(\gamma)$ from threshold to an energy of 3 GeV, using events with Initial State Radiation (ISR) collected with the BABAR detector, is presented. The ISR luminosity is determined from a study of the leptonic process $e^+e^- \rightarrow \mu^+\mu^-\gamma(\gamma)$, and the method is tested by the comparison with the next-to-leading order (NLO) QED prediction. The leading-order hadronic contribution to the muon magnetic anomaly calculated using the BABAR $\pi\pi$ cross section measured from threshold to 1.8 GeV is $(514.1 \pm 2.2(\text{stat}) \pm 3.1(\text{syst})) \times 10^{-10}$. Other results on ISR multihadronic cross sections from BABAR are presented.

1. Introduction

The measurements of the $e^+e^- \rightarrow$ hadrons cross-section are used to evaluate dispersion integrals for calculations of the hadronic vacuum polarization (VP). In particular, the hadronic contribution to the muon magnetic moment anomaly (a_μ^{had}) requires data in the low mass region, dominated by the process $e^+e^- \rightarrow \pi^+\pi^-(\gamma)$ which provides 73% of the contribution. The dominant uncertainty comes also from the $\pi\pi$ channel.

The systematic precision of the (recent) previously measured $\pi\pi$ cross sections is of 0.8% for CMD2 [2] and 1.5% for SND [3], the two measurements being in good agreement. The first ISR measurement done by KLOE [4] had a quoted systematic precision of 1.3%, and some deviation in shape was observed when comparing to the Novosibirsk data. For the reanalysed KLOE data [5] a systematic uncertainty of 0.9% is quoted, and the agreement with the Novosibirsk data is improved.

The comparison of the theoretical and measured [1] values of a_μ shows a discrepancy of about 3σ when previous e^+e^- data [2,3,5] are used, possibly hinting at new physics. An ap-

proach using τ decay data corrected for isospin-breaking, leads to a smaller difference [7].

The BABAR 2π results presented in these proceedings were published in [8]. Their achieved goal was to obtain a measurement of the contribution of the 2π channel to (a_μ^{had}) with a precision better than 1%, implying a control of systematic uncertainties at the 10^{-3} level.

2. The BABAR ISR $\pi\pi$ analysis

The results on the $\pi\pi$ cross section presented here are obtained with the ISR method [6] using e^+e^- annihilation events collected with the BABAR detector, at a center-of-mass energy \sqrt{s} near 10.58 GeV. We consider events $e^+e^- \rightarrow X\gamma_{\text{ISR}}$, where X includes any final state, and the ISR photon is emitted by the e^+ or e^- . The $e^+e^- \rightarrow \pi\pi(\gamma_{\text{FSR}})$ cross section is obtained as a function of $\sqrt{s'}$, which is the invariant mass of the final state. The advantage of the ISR method is that all the mass spectrum is covered at once (from threshold to 3 GeV in BABAR) with the same detector conditions and analysis.

In the BABAR analysis the $\pi^+\pi^-\gamma_{\text{ISR}}(\gamma_{\text{FSR}})$ and $\mu^+\mu^-\gamma_{\text{ISR}}(\gamma_{\text{FSR}})$ spectra are measured. This is the first NLO measurement, an eventual additional radiation being taken into account in

*Now at CERN, CH-1211, Geneva 23, Switzerland.

the analysis, instead of being corrected a posteriori (as done by previous experiments). The muon spectrum is compared with the NLO QED prediction, this important cross check of the analysis being called the QED test. The $\sqrt{s'}$ spectrum of $e^+e^- \rightarrow X\gamma$ events is related to the cross section for the process $e^+e^- \rightarrow X$ through

$$\frac{dN_{X\gamma}}{d\sqrt{s'}} = \frac{dL_{ISR}^{eff}}{d\sqrt{s'}} \varepsilon_{X\gamma}(\sqrt{s'}) \sigma_X^0(\sqrt{s'}), \quad (1)$$

where $\varepsilon_{X\gamma}$ is the detection efficiency (acceptance) determined by simulation with corrections obtained from data, and σ_X^0 is the bare cross section (excluding VP). The muon spectrum is used to derive the effective ISR luminosity L_{ISR}^{eff} . We correct for the leading order FSR contribution for muons (smaller than 1%, below 1 GeV), while additional FSR photons are measured. The $\pi\pi(\gamma_{FSR})$ cross section is obtained from the ratio of the 2π spectrum and L_{ISR}^{eff} , where the e^+e^- luminosity, additional ISR effects, vacuum polarization and ISR photon efficiency cancel, hence the strong reduction of the systematic uncertainty.

This analysis is based on 232 fb^{-1} of data recorded with the BABAR detector [9] at the PEP-II asymmetric-energy e^+e^- storage rings. Charged-particle tracks are measured with a five-layer double-sided silicon vertex tracker (SVT) together with a 40-layer drift chamber (DCH) inside a 1.5 T superconducting solenoid magnet. The energy and direction of photons are measured in the CsI(Tl) electromagnetic calorimeter (EMC). Charged-particle identification (PID) uses ionization loss dE/dx in the SVT and DCH, the Cherenkov radiation detected in a ring-imaging device (DIRC), and the shower deposit in the EMC (E_{cal}) and in the instrumented flux return (IFR) of the magnet.

Two-body ISR events are selected by requiring a photon with $E_\gamma^* > 3 \text{ GeV}$ and laboratory polar angle in the range $0.35 - 2.4 \text{ rad}$, and exactly two tracks of opposite charge, each with momentum $p > 1 \text{ GeV}/c$ and within the angular range $0.40 - 2.45 \text{ rad}$. Events with one single charged track are also recorded and exploited for efficiency measurements.

Signal and background ISR processes are simulated with Monte Carlo (MC) event genera-

tors based on Ref. [10]. Additional ISR photons are generated with the structure function method [11], and additional FSR photons with PHOTOS [12]. The response of the BABAR detector is simulated with GEANT4 [14].

Background events from $e^+e^- \rightarrow q\bar{q}$ ($q = u, d, s, c$) are generated with JETSET [13]. They are due to low-multiplicity events in which an energetic γ originating from a π^0 is mistaken as the ISR photon candidate. To normalize this rate from JETSET, the π^0 yield (obtained by pairing the ISR photon with other photons in the event) is compared in data and MC. Multi-hadronic ISR backgrounds are dominated by $e^+e^- \rightarrow \pi^+\pi^-\pi^0\gamma$ and $e^+e^- \rightarrow \pi^+\pi^-2\pi^0\gamma$ contributions. An approach similar to that for $q\bar{q}$ is followed to calibrate the background level from the 3π ISR process, using ω and ϕ signals. The MC estimate for the $2\pi 2\pi^0\gamma$ process is used and assigned a 10% systematic uncertainty. Background contributions to the $\mu\mu$ spectrum are found to be negligible.

Acceptance and mass-dependent efficiencies for trigger, reconstruction, PID, and event selection are computed using the simulation. The ratios of data and MC efficiencies have been determined from specific studies, as described below, and are applied as mass-dependent corrections to the MC efficiency. They amount to at most a few percent and are known to a few permil level or better.

Tracking and PID efficiencies are determined taking advantage of pair production. For tracking studies, two-prong ISR candidates are selected on the basis of the ISR photon and one track. A kinematic fit yields the expected parameters of the second track. The unbiased sample of candidate second tracks is used to measure track reconstruction efficiency. The study of 2-particle overlap in the detector required a large effort to reach the per mil accuracies.

Each event is subjected to two kinematic fits to the $e^+e^- \rightarrow X\gamma$ hypothesis, where X allows for possible additional radiation. Both fits use the ISR photon direction and the parameters and covariance matrix of each charged-particle track. The two-constraint (2C) ‘ISR’ fit allows an undetected photon collinear with the collision axis, while the 3C ‘FSR’ fit is performed only when

an additional photon is detected. Most events have small χ^2 values for both fits; an event with only a small χ_{ISR}^2 (χ_{FSR}^2) indicates the presence of additional ISR (FSR) radiation. Events where both fits have large χ^2 values result from track or ISR photon resolution effects, the presence of additional radiated photons, or multi-hadronic background. To accommodate the expected background levels, different criteria in the $(\chi_{ISR}^2, \chi_{FSR}^2)$ plane are applied, i.e. a loose 2D cut in the central ρ region and a tighter cut for the ρ tails. The loose cut is also used in the $\mu\mu\gamma$ analysis. The $\pi\pi$ ($\mu\mu$) mass is calculated from the best ‘ISR’ or ‘FSR’ fit.

The computed acceptance and the χ^2 selection efficiency depend on the description of radiative effects in the generator. The difference of the FSR rate between data and MC is measured, resulting in a small correction for the cross section. More significant differences are found between data and the generator for additional ISR photons, since the latter uses a collinear approximation and an energy cut-off for very hard photons. Induced kinematical effects have been studied using the NLO PHOKHARA generator [15] at four-vector level with fast simulation. Differences occurring in acceptance yield corrections to the QED test. In contrast, since radiation from the initial state is common to the pion and muon channels, the $\pi\pi(\gamma)$ cross section, obtained from the $\pi\pi/\mu\mu$ ratio, is affected and corrected only at a few permil level. The χ^2 selection efficiency determined from muon data applies to pions, after correction for the effect of secondary interactions and the π/μ difference for additional FSR. The measured $\pi\pi(\gamma)$ cross section is to a large extent insensitive to the description of NLO effects in the generator.

3. The QED test

The QED test involves two additional factors, both of which cancel in the $\pi\pi/\mu\mu$ ratio: L_{ee} and the ISR photon efficiency, which is measured using a $\mu\mu\gamma$ sample selected only on the basis of the two muon tracks. The QED test is expressed as the ratio of data to the simulated spectrum, after the latter is corrected using data for all known detector and reconstruction differences. The gen-

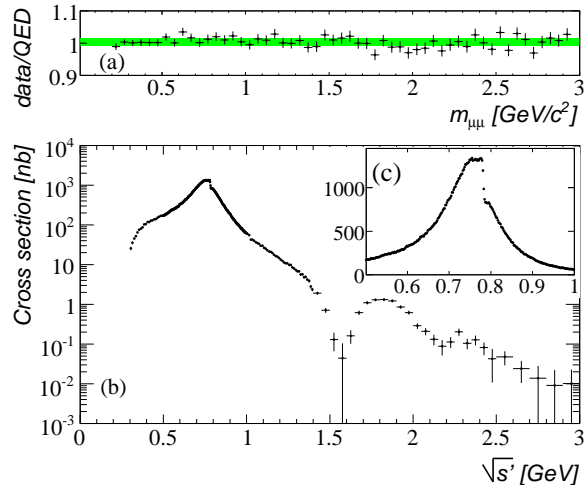


Figure 1. (a) The ratio of the measured cross section for $e^+e^- \rightarrow \mu^+\mu^-\gamma(\gamma)$ to the NLO QED prediction. The band represents Eq. (2). (b) The measured cross section for $e^+e^- \rightarrow \pi^+\pi^-\gamma(\gamma)$ from 0.3 to 3 GeV. (c) Enlarged view of the ρ region in energy intervals of 2 MeV. The plotted errors are from the sum of the diagonal elements of the statistical and systematic covariance matrices.

erator is also corrected for its known NLO deficiencies using the comparison to PHOKHARA. The ratio is consistent with unity from threshold to 3 GeV/c^2 , (Fig. 1 (a)). A fit to a constant value yields $(\chi^2/n_{\text{df}} = 55.4/54; n_{\text{df}} = \text{number of degrees of freedom})$

$$\frac{\sigma_{\mu\mu\gamma(\gamma)}^{\text{data}}}{\sigma_{\mu\mu\gamma(\gamma)}^{\text{NLO QED}}} - 1 = (40 \pm 20 \pm 55 \pm 94) \times 10^{-4}, \quad (2)$$

where the errors are statistical, systematic from this analysis, and systematic from L_{ee} (measured using Bhabha scattering events), respectively. The QED test is thus satisfied within an overall accuracy of 1.1%.

4. Angular distribution in the $\pi\pi$ center-of-mass

The pion angular distribution in the $\pi\pi$ center-of-mass with respect to the ISR photon direction

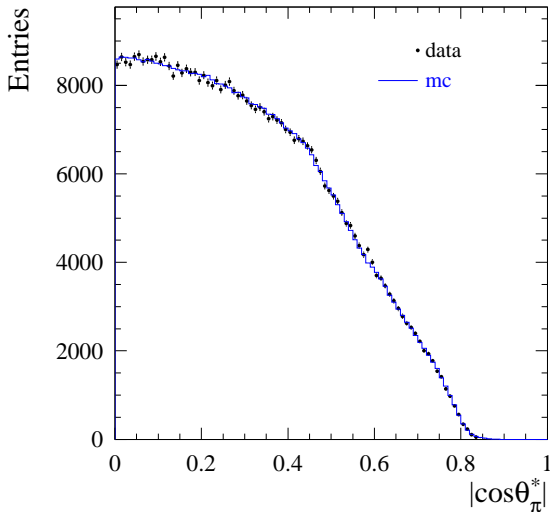


Figure 2. The angular pion distribution in the $\pi\pi$ system with respect to the ISR photon direction as function of $|\cos\theta_\pi^*|$ for background-subtracted $\pi\pi\gamma(\gamma)$ data (points) in the ρ central region ($0.5 < m_{\pi\pi} < 1 \text{ GeV}/c^2$). The blue histogram is the shape obtained in the simulation, normalized to the data.

in that frame, is model-independent. The $\cos\theta_\pi^*$ distribution behaves as $\sin^2\theta_\pi^*$ as a consequence of the P-wave between the two pions, but it is strongly distorted at $|\cos\theta_\pi^*|$ values near one due to the $p > 1 \text{ GeV}/c$ cut on the tracks.

The $|\cos\theta_\pi^*|$ distributions for background-subtracted data and MC are compared in Fig. 2 for the $0.5 - 1 \text{ GeV}/c^2$ mass range: they agree with each other within the statistical uncertainties, as expected for a pure pion sample.

5. The $\pi\pi$ cross section

To correct for resolution and FSR effects, an unfolding of the background-subtracted $m_{\pi\pi}$ distribution, corrected for data/MC efficiency differences, is performed. A mass-transfer matrix, created using simulation, provides the probability that an event generated in a $\sqrt{s'}$ interval i is reconstructed in a $m_{\pi\pi}$ interval j . The ma-

Table 1

Relative systematic uncertainties (in 10^{-3}) on the $e^+e^- \rightarrow \pi^+\pi^-(\gamma)$ cross section by $\sqrt{s'}$ intervals (in GeV) up to 1.2 GeV. The statistical part of the efficiency uncertainties is included in the total statistical uncertainty in each interval.

Source of Uncertainty	$\sqrt{s'}$ (GeV)				
	0.3-0.4	0.4-0.5	0.5-0.6	0.6-0.9	0.9-1.2
trigger/ filter	5.3	2.7	1.9	1.0	0.5
tracking	3.8	2.1	2.1	1.1	1.7
π -ID	10.1	2.5	6.2	2.4	4.2
background	3.5	4.3	5.2	1.0	3.0
acceptance	1.6	1.6	1.0	1.0	1.6
kinematic fit (χ^2)	0.9	0.9	0.3	0.3	0.9
correlated $\mu\mu$ ID loss	3.0	2.0	3.0	1.3	2.0
$\pi\pi/\mu\mu$ non-cancel.	2.7	1.4	1.6	1.1	1.3
unfolding	1.0	2.7	2.7	1.0	1.3
ISR luminosity ($\mu\mu$)	3.4	3.4	3.4	3.4	3.4
total uncertainty	13.8	8.1	10.2	5.0	6.5

trix is corrected to account for the larger fraction of events with bad χ^2 values (and consequently poorer mass resolution) in data compared to MC because of the approximate simulation of additional ISR. The performance and robustness of the unfolding method [16] have been assessed using test models.

The results for the $e^+e^- \rightarrow \pi^+\pi^-(\gamma)$ bare cross section including FSR, $\sigma_{\pi\pi(\gamma)}^0(\sqrt{s'})$, are given in Fig. 1 (b). Prominent features are the dominant ρ resonance, the abrupt drop at 0.78 GeV due to ρ - ω interference, a clear dip at 1.6 GeV resulting from higher ρ state interference, and some additional structure near 2.2 GeV. Systematic uncertainties are reported in Table 1 for $0.3 < \sqrt{s'} < 1.2 \text{ GeV}$. Although larger outside this range, they do not exceed statistical errors over the full spectrum for the chosen energy intervals. In particular, a systematic uncertainty of only 0.5% has been achieved in the central ρ region.

The BABAR data were compared to other experiments, exploiting a VDM fit of the pion form factor [17]. This fit describes well the BABAR data in the region of interest for the comparison. There is a relatively good agreement when comparing to the Novosibirsk data [2,3] in the ρ mass region, while a slope is observed when comparing to the KLOE '08 data [5]. A flatter shape is observed when comparing to the re-

cent KLOE [18] data, obtained by the analysis of events with a detected, large angle ISR photon. A good agreement is observed when comparing to the Novosibirsk and KLOE data, in the low mass region, below $0.5 \text{ GeV}/c^2$. There is a good agreement between the BABAR data and the most recent τ data (corrected for isospin-breaking effects) from Belle [19], while some systematic effects are observed when comparing to ALEPH [20] and CLEO [21].

6. The $\pi\pi$ contribution to a_μ

The lowest-order contribution of the $\pi\pi(\gamma)$ intermediate state to the muon magnetic anomaly is given by

$$a_\mu^{\pi\pi(\gamma),LO} = \frac{1}{4\pi^3} \int_{4m_\pi^2}^{\infty} ds' K(s') \sigma_{\pi\pi(\gamma)}^0(s'), \quad (3)$$

where $K(s')$ is a known kernel [22]. The integration uses the measured cross section and the errors are computed using the full statistical and systematic covariance matrices. The systematic uncertainties for each source are taken to be fully correlated over the full mass region. The integrated result from threshold to 1.8 GeV is

$$a_\mu^{\pi\pi(\gamma),LO} = (514.1 \pm 2.2 \pm 3.1) \times 10^{-10}, \quad (4)$$

where the errors are statistical and systematic. This value is larger than that from a combination of previous e^+e^- data [7] (503.5 ± 3.5), but is in good agreement with the updated value from τ decay [7] (515.2 ± 3.4). The deviation between the BNL measurement [1] and the theoretical prediction is reduced to 2.4 standard deviations, when using the $\pi^+\pi^-$ data from BABAR only.

7. Other ISR measurements from BABAR

Many other ISR measurements [23,24,25,26,27] have been published by BABAR in the past (see Fig. 3). They have an improved precision comparing to previous measurements. Still more channels are under analysis: K^+K^- , $K\bar{K}\pi\pi$ including K^0 's, and $\pi^+\pi^-2\pi^0$. The last one is especially important in order to clarify the existing discrepancy between the e^+e^- and τ -based contributions to a_μ from this channel [28].

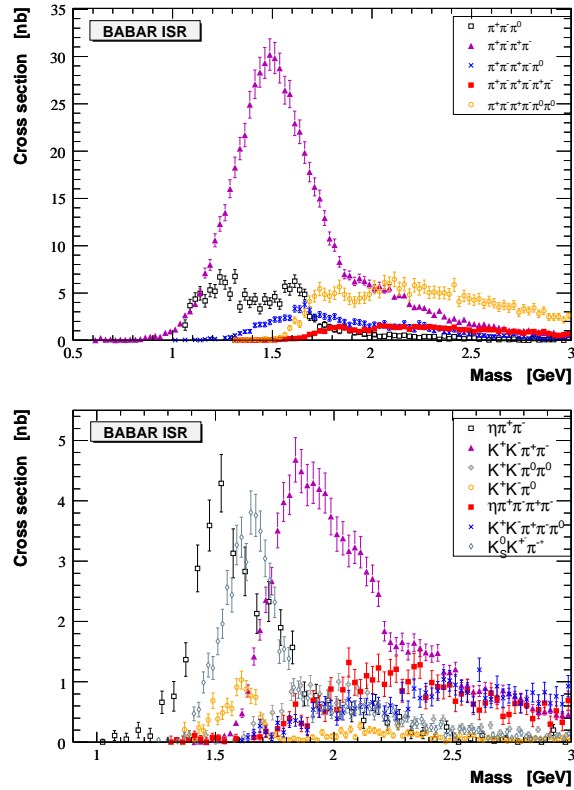


Figure 3. Cross sections obtained by BABAR using the ISR method. The error bars include statistical and systematic uncertainties added in quadrature.

8. Conclusions and perspectives

BABAR has analyzed the $\pi^+\pi^-$ and $\mu^+\mu^-$ ISR processes in a consistent way, on the full mass range of interest ($0.3 - 3 \text{ GeV}/c^2$). In addition, the absolute $\mu^+\mu^-$ cross section has been compared to the NLO QED prediction, the two being in agreement within 1.1%. The $e^+e^- \rightarrow \pi^+\pi^-(\gamma)$ cross section, obtained through the ratio of the $\pi^+\pi^-$ and $\mu^+\mu^-$ spectra is rather insensitive to the detailed description of radiation in MC. A strong point of the present analysis, comparing to previous ISR studies, comes from the fact that several uncertainties cancel in this ratio, allowing us to achieve our precision goal:

the systematic uncertainty in the central ρ region ($0.6 - 0.9 \text{ GeV}/c^2$) is only 0.5%.

The contribution to a_μ from the BABAR $\pi^+\pi^-$ spectrum, in the range $0.28 - 1.8 \text{ GeV}$, is $(514.1 \pm 2.2 \pm 3.1) \times 10^{-10}$. This result has a precision of 0.7%, comparable to the combined previous measurements. The contribution from multi-hadronic channels will continue to be updated, with more results forthcoming from BABAR.

In the comparison between the BABAR $\pi^+\pi^-(\gamma)$ cross section and the data from other experiments, there is a fair agreement with CMD2 and SND, while the agreement is poor when comparing with KLOE. The first priority should be to clarify the BABAR/KLOE discrepancy, the most important effect on a_μ being due to the difference on the ρ peak. The origin of the slope in this comparison is also to be understood. The slope was very pronounced when comparing with the 2004 KLOE results, and it is reduced with the 2008 and 2010 data. The same slope is also observed in the comparison of the KLOE and τ data, while BABAR is in good agreement with the τ results. Further checks of the KLOE results are possible. Actually, as the method is based on MC simulation for ISR and additional ISR/FSR probabilities, an important cross-check should be provided by the comparison of the $\mu\mu$ spectrum with the QED prediction.

REFERENCES

1. G.W. Bennett *et al.*, Phys. Rev. **D73**, 072003 (2006).
2. V.M. Aulchenko *et al.*, JETP Lett. **82**, 743 (2005); JETP Lett. **84**, 413 (2006); R.R. Akhmetshin *et al.*, Phys. Lett. **B648**, 28 (2007).
3. M.N. Achasov *et al.*, JETP **103**, 380 (2006).
4. KLOE Collaboration (F. Aloisio *et al.*), Phys. Lett. **B606**, 12 (2005).
5. KLOE Collaboration (F. Ambrosino *et al.*), Phys. Lett. **B670**, 285 (2009).
6. A.B. Arbuzov *et al.*, J. High Energy Phys. **9812**, 009 (1998); S. Binner, J.H. Kühn, and K. Melnikov, Phys. Lett. **B459**, 279 (1999).
7. M. Davier *et al.*, Eur. Phys. J. C **66**, 127 (2010).
8. B. Aubert *et al.* [BABAR Collaboration], Phys. Rev. Lett. **103**, 231801 (2009).
9. B. Aubert *et al.*, Nucl. Instr. Meth. **A479**, 1 (2002).
10. H. Czyż and J.H. Kühn, Eur. Phys. J. **C18**, 497 (2001).
11. M. Caffo, H. Czyż, and E. Remiddi, Nuo. Cim. **110A**, 515 (1997).
12. E. Barberio, B. van Eijk, and Z. Was, Comput. Phys. Comm. **66**, 115 (1991).
13. T. Sjöstrand, Comput. Phys. Commun. **82**, 74 (1994).
14. S. Agostinelli *et al.*, Nucl. Instr. Meth. **A506**, 250 (2003).
15. H. Czyż *et al.*, Eur. Phys. J. **C35**, 527 (2004); Eur. Phys. J. **C39**, 411 (2005).
16. B. Malaescu, arXiv:0907.3791, sub. to Nucl. Instr. Meth..
17. B. Malaescu's slides at this workshop.
18. KLOE Collaboration (F. Ambrosino *et al.*), arXiv:1006.5313 (2010).
19. Belle Collaboration (M. Fujikawa *et al.*), Phys. Rev. **D78**, 072006 (2008).
20. ALEPH Collaboration (S. Schael *et al.*), Phys. Rep. **421**, 191 (2005).
21. CLEO Collaboration (S. Anderson *et al.*), Phys. Rev. **D61**, 112002 (2000).
22. S.J. Brodsky and E. de Rafael, Phys. Rev. **168**, 1620 (1968).
23. BABAR Collaboration (B. Aubert *et al.*), Phys. Rev. **D71**, 052001 (2005).
24. BABAR Collaboration (B. Aubert *et al.*), Phys. Rev. **D73**, 052003 (2006).
25. BABAR Collaboration (B. Aubert *et al.*), Phys. Rev. **D76**, 012008 (2007).
26. BABAR Collaboration (B. Aubert *et al.*), Phys. Rev. **D76**, 092005 (2007), Erratum-ibid. **D77**, 119902 (2008).
27. BABAR Collaboration (B. Aubert *et al.*), Phys. Rev. **D77**, 092002 (2008).
28. M. Davier, A. Hoecker, B. Malaescu, C. Z. Yuan and Z. Zhang, Eur. Phys. J. C **66**, 1 (2010).